Journal Pre-proof

The birth of the Gondwanide arc: Insights into Carboniferous magmatism of the North Patagonian Andes (Argentina)

María Belén Yoya, Sebastián Oriolo, Pablo González, Florencia Restelli, Emiliano Renda, Florencia Bechis, Jerónimo Christie Newbery, Paulo Marcos, Ezequiel Olaizola

PII: S0895-9811(23)00036-6

DOI: https://doi.org/10.1016/j.jsames.2023.104225

Reference: SAMES 104225

To appear in: *Journal of South American Earth Sciences*

Received Date: 21 November 2022

Revised Date: 25 January 2023

Accepted Date: 26 January 2023

Please cite this article as: Yoya, Marí.Belé., Oriolo, Sebastiá., González, P., Restelli, F., Renda, E., Bechis, F., Newbery, Jeró.Christie., Marcos, P., Olaizola, E., The birth of the Gondwanide arc: Insights into Carboniferous magmatism of the North Patagonian Andes (Argentina), *Journal of South American Earth Sciences* (2023), doi: https://doi.org/10.1016/j.jsames.2023.104225.

The birth of the Gondwanide arc: Insights into Carboniferous magmatism of the North Patagonian Andes (Argentina)

María Belén Yoya[a*], Sebastián Oriolo[a], Pablo González[b], Florencia Restelli[a], Emiliano Renda[c], Florencia Bechis[d], Jerónimo Christie Newbery[e], Paulo Marcos[c], Ezequiel Olaizola[d]

[a] CONICET-Universidad de Buenos Aires. Instituto de Geociencias Básicas, Aplicadas y Ambientales de Buenos Aires (IGEBA), Intendente Guiraldes 2160, C1428EHA Buenos Aires, Argentina.

[b] CONICET-SEGEMAR, Regional Sur, Independencia 1495, Parque Industrial 1, R8332EXZ, General Roca, Argentina.

[c] Instituto de Investigación en Paleobiología y Geología (UNRN-CONICET), Avenida Julio A. Roca 1242, R8332EXZ, General Roca, Argentina.

[d] Universidad Nacional de Río Negro, Instituto de Investigaciones en Diversidad Cultural y Procesos de Cambio (UNRN-CONICET), Bartolomé Mitre 630, R8400AHN San Carlos de Bariloche, Argentina.

[e] Departamento de Ciencias Geológicas, Universidad de Buenos Aires, Intendente Güiraldes 2160, C1428EHA, Buenos Aires, Argentina.

* Corresponding author: belen.yoya@gmail.com

Abstract

New geological, structural, and geochemical information was obtained for the late Paleozoic basement of the North Patagonian Andes. The studied rocks are mainly formed by foliated diorites and gabbro-diorites with a primitive continental arc signature, according to trace elements patterns. Similar petrological and structural characteristics, together with previously reported ages between ca. 330 and 323 Ma, permit the correlation of these rocks with plutonic bodies located in the North Patagonian Andes, North Patagonian Massif and Cordillera de la Costa of Chile, documenting the onset of Gondwanide subduction along the proto-Pacific margin of Gondwana between ca. 37 and 45°S. Geochemical and geochronological data, together with field evidence, suggest mafic magma replenishment during the construction of this large batholith. The presence of sheeted zones and magmatic fabrics allow to interpret pluton emplacement in a highly coupled system linked with a tectonically active setting, under pressure conditions of ca. 6 ± 1 Kbar.

Keywords: Primitive arc melts, Gondwanide orogeny, Late Paleozoic, sheeted zones, Western Gondwana.

1. Introduction

Subduction-related magmatism occurs in the upper continental plate of convergent margins, driven by dehydration reactions in the downgoing slab (Gill, 1981) and the ascent of melange diapirs (Marschall and Schumacher, 2012). The magmatism formed above subduction zones is thus characterized by significant amounts of volatiles and has an extensive range of silica contents, calc-alkaline compositions, and distinct trace element patterns. The great majority of Cordilleran batholiths are intermediate (tonalite to granodiorite) in composition, whereas gabbroic intrusions are subordinate and more common during primitive stages of arc construction (e.g., Schmidt and Jagoutz, 2017). Therefore, arc magmatism requires additional controls during its evolution, such as magmatic differentiation, fractional crystallization, host rock assimilation, partial melting, or a combination of them. All these processes can generate silica enrichment, resulting in modified geochemical trends from a primary mantle source (Ducea et al., 2015 and references therein).

The Gondwanide orogeny comprises one of the most exceptional tectono-magmatic records of the Earth history (e.g., Cawood et al., 2011). In southern South America, the beginning of this orogeny is characterized by an active continental arc built along the proto-Andean margin (Llambías et al., 1993; Pankhurst et al., 2006; Dahlquist et al., 2018). However, the Gondwanide magmatism shows a protracted evolution from the late Mississippian to the Triassic south of 39° (Llambías et al., 1984; Sato et al., 2015; Alasino et al., 2022). This evolution is particularly well-documented in the Patagonian region, where Carboniferous to late Permian intrusions monitor spatio-temporal variation of arc dynamics (e.g., Pankhurst et al., 2006; Varela et al., 2005, 2015; Oriolo et al., 2022).

This work focuses on Carboniferous magmatism exposed in the North Patagonian Andes between the Guillelmo lake region and the Cordón del Serrucho. Geological, geochemical, barometric, structural, and microstructural data are integrated to characterize their nature and petrogenesis. In addition, the tectonomagmatic setting in the context of the Gondwanide arc dynamics along the southwestern Gondwana margin is assessed.

2. Geological setting

In southern South America, the Gondwanide magmatism is well-documented and has been defined as different igneous cycles between the Late Paleozoic and Late Triassic (Llambías et al., 1984; Sato et al., 2015; Gregori et al., 2020; Alasino et al., 2022). The beginning of this cycle is recorded along discontinuous pre-Andean outcrops (e.g., Llambías et al., 1993; Alasino et al., 2012; del Rey et al., 2016; Dahlquist et al., 2018, 2021). Particularly, the Paleozoic magmatism in northwestern Patagonia, is exposed between the North Patagonian Cordillera and the North Patagonian Massif (Fig. 1 and Table 1; Varela et al., 2005). In the former, middle to late Carboniferous magmatism crops out in the Cordón del Serrucho and further south at Cañadón de la Mosca, and is considered part of the Colohuincul Complex (Giacosa et al., 2001; Varela et al., 2005, 2015; Pankhurst et al., 2006). During the Permian and Triassic, widespread igneous activity continued, evolving from calc-alkaline orogenic associations to alkaline postorogenic sequences (e.g., Pankhurst et al., 2006). Permian magmatism in the western North Patagonian Massif corresponds to the Mamil Choique Formation and is exposed near Piedra del Águila and the Sierra Mamil Choique (Volkheimer, 1964; Ravazzoli and Sesana, 1977; Proserpio, 1978; Cerredo and López de Luchi, 1998; Varela et al., 2005, 2015; Pankhurst et al., 2006).

In the southwestern Gondwana region, the Gondwanide magmatism is part of the igneous-metamorphic northern Patagonian basement, including both magmatic foliated and non-foliated facies. It occurs together with metasedimentary sequences, as in the case of the Colohuincul Complex (Dalla Salda et al., 1991; García-Sansegundo et al., 2009). In general, the late Carboniferous-Permian magmatism exhibits dominantly calc-alkaline trends, meta- to peraluminous, and I- to S-type compositions (Varela et al., 2005, 2015; Pankhurst et al., 2006). Notably, the North Patagonian Andes basement between the Mascardi lake in the north and the Cordón del Serrucho to the south presents significant exposures of Carboniferous igneous-metamorphic basement rocks (Figs. 1 and 3). However, these rocks have alternatively been attributed to either Late Carboniferous intrusions or amphibolites/metasedimentary sequences of the Colohuincul Complex (Dalla Salda et al., 1991; Giacosa and Heredia, 2001; Varela et al., 2005, 2015; Pankhurst et al., 2006; García-Sansegundo et al., 2009).

In the southeastern North Patagonian Massif (Fig. 1), Late Carboniferous magmatism corresponds to the El Platero tonalite, with an age of 329 ± 4 Ma (Fig. 1; Pankhurst et al., 2006). Likewise, Late Carboniferous magmatism was also identified in Paso del Sapo and Sierra de los Pichiñanes, with ages of 314 ± 2 and 318 ± 2 Ma, respectively (Pankhurst et al., 2006; Renda et al., 2021). Finally, Permian magmatism is also present in the region, with Cisuralian intrusions such as the El Tunel tonalite in Río Chico (295 ± 2 Ma), the Laguna del Toro granodiorite near Gastre (294 ± 3 Ma), and the Mamil Choique Formation (281 ± 2 Ma) in the homonymous range (Varela et al., 2005; Pankhurst et al., 2006).

Further north, Late Paleozoic magmatism is present in the Precordillera Neuquina, as indicated by the Chachil Plutonic Complex, which intrudes the Piedra Santa metasedimentary complex and yields U-Pb zircon ages of 303 ± 2 Ma, 300 ± 2 Ma, 305 ± 2 Ma, and 358 ± 2 Ma (Franzese, 1995; Romero et al., 2019; Oriolo et al., 2022). Based on petrological and age similarities, the Chachil Plutonic Complex can be correlated with coeval plutons of the Coastal Batholith of Chile between 37 and 41°S (Hervé et al., 1984; Varela et al., 1994; Franzese, 1995; Romero et al., 2019).

At the southern North Patagonian Cordillera, in the Cordón del Serrucho area, Carboniferous biotite- and hornblende-bearing foliated granodiorites present a U-Pb SHRIMP zircon age of 330 ± 4 Ma (Pankhurst et al., 2006). In addition, comparable intrusions yielded U-Pb ages of 324 ± 2 Ma (Oriolo et al., 2022) and 323 ± 3 Ma (Varela et al., 2005, 2015; Pankhurst et al., 2006) at Morro de Sheffield and Cañadón de la Mosca areas, respectively.

The basement rocks of the Guillelmo lake study area (Fig. 1) were first described as diorite igneous bodies (Feruglio, 1941) and then as amphibolites assigned to the Colohuincul Complex with K-Ar hornblende ages of 344 ± 30 and 329 ± 24 Ma (Dalla Salda et al., 1991; García-Sansegundo et al., 2009). Recent U-Pb LA-ICP-MS zircon analyses on the diorites yielded an age of 325 ± 4 Ma (Oriolo et al., 2022). Consequently, these basement rocks have an ambiguous interpretation, similar to those exposed further south in the Cañadón de la Mosca, which have alternatively been described as amphibolites or diorites-tonalites (Varela et al., 2005; Pankhurst et al., 2006).

3. Methodology

Geological and structural mapping was carried out by combining Landsat 8 image processing with new field data (Fig. 2) and published maps (González Bonorino, 1944; Feruglio, 1947; Dalla Salda et al., 1991; Giacosa and Heredia, 2001; García-Sansegundo et al., 2009). Fieldwork included structural data collection and sampling for petrographic and geochemical analysis. Structural data were processed with Stereonet (Allmendinger et al., 2012; Cardozo et al., 2013).

For geochemical characterization, whole-rock analyses were carried out at AcmeLabs, Canada (http://acmelab.com/) for major, trace, and rare earth elements using lithoborate fusion and ICP-MS methods. Results of the new geochemical data are exhibited in Supplementary

Material_1. Data analysis, including analyses published by Dalla Salda et al. (1991), Pankhurst et al. (2006), García-Sansegundo et al. (2009), and Varela et al. (2015), was carried out with GCDKit 6.0 (Janousek et al., 2006, 2016). Although García-Sansegundo et al. (2009) also reported analysis of granitic bodies, these were not included due to mapping criteria, as they may likely be of Jurassic age (e.g., Castro et al., 2011).

Additionally, a J EOL JXA-8530F electron probe microanalyzer at the Institute of Earth Science of the University of Lausanne (Switzerland) was used to acquire quantitative analyses of amphiboles. Spot analyses were performed using an accelerating voltage of 15 keV. To avoid electron-beam induced decomposition of amphibole that normally contains volatile elements, a current of 15 nA was applied for. A beam size ranging between 2 and 5 μm was used depending on the size of the mineral. Al-in-Hornblende barometric estimations were based on the calibrations of Schmidt et al. (1992) and Mutch et al. (2016). Analytical results are shown in Supplementary Material_2.

4. Results

4.1 Lithological characterization

Carboniferous igneous rocks of the study area are grouped in a batholith of at least ca. 300 km^2, elongated in a NNW-SSE direction (Fig. 2). At the Guillelmo lake area, it consists of magmatic foliated diorites and subordinate foliated quartz-diorites, tonalites, and gabbros (Fig. 3A), being comparable those exposed in the Cañadón de la Mosca (Fig. 3B). Further south, more felsic rocks are generally dominant in the Cordón del Serrucho, corresponding mainly to diorites and quartz-diorites, whereas intercalated diorites and gabbros crop out at the southernmost exposures at the Morro de Sheffield. Microgranular mafic enclaves are frequent in all these rocks (Fig. 3C).

All rocks typically include magmatic structures. Magmatic foliation and lineation are well-defined by the shape-preferred orientation of euhedral amphibole and plagioclase. Parallel to the foliation, compositional layering with gabbro to diorite/tonalite alternating bands is common (Fig. 3D-E). In some cases, this layering defines areas of sheeted plutons and schlieren (Fig. 3F). When present, elongated microgranular enclaves are often parallel to the foliation. However, local high-temperature solid-state fabrics resulting in dioritic orthogneisses were recorded as well, mainly at the northeastern margin of the pluton close to the contact with the country rocks and also locally in different sectors of the pluton.

The country rocks of the batholith are exposed at the northeastern part of Guillelmo lake. It consists of paragneisses, schists, and minor amphibolites with a dominantly WNW-ESE-striking foliation, which dips moderately to the SSW. The intrusive contact is poorly exposed, as pluton margins are mainly overprinted by younger Jurassic intrusions or covered by vegetation or Cenozoic sequences.

4.2 Structure

The magmatic foliation of rocks is nearly ubiquitous and lies parallel to the compositional layering and trails of elongated enclaves, which are present in some cases (Fig. 3). These fabrics are dominantly oriented in NNW-SSE to WNW-ESE direction (Fig. 2). At the Guillelmo lake, the foliation strikes NNW-SSE to NW-SE and shows mainly moderate to gentle dips towards the SSW/SW. The orientation of associated lineations is more scattered, plunging either gently to the SE or moderately to the WSW-NW. At the Cañadón de la Mosca, the magmatic foliation strikes NNW-SSE and moderately dips to the ENE. In the case of Cordón del Serrucho and Morro de Sheffield, a NW-SE to WNW-ESE-striking foliation is documented, with moderate to steep dips to the SSW/SW and NNE/NE, though the former seems to be dominant. Moderate to gentle plunge toward the S/SSE characterizes lineations. Besides structures that describe the internal fabric of the body, igneous rocks are cross-cut by ductile to brittle-ductile shear zones and faults, at outcrop scale. Shear zones comprise mylonitic bands exposed at the western margin of the Guillelmo lake, overprinting dioritic rocks, which are cross-cut by late fault zones.

4.3 Petrography and microstructures

The rocks of the study area correspond to amphibole ± biotite quartz-diorites, diorites, and subordinate gabbros, according to the QAP diagram of plutonic rocks (Le Maitre, 2002; Fig. 4A-B). Apatite, titanite, rutile, zircon, magnetite and other opaque minerals are accessory minerals. Alteration to epidote and chlorite is also observed in some cases.

Amphibole and plagioclase crystals are aligned, defining a shape-preferred orientation (Fig. 4A). As observed in the field, the magmatic layering is also evidenced at microscopic scale, documented by alternating mafic and felsic bands of variable grain sizes (Fig. 4B).

Likewise, the rocks record other magmatic features, such as zoned euhedral plagioclase crystals (e.g., Paterson et al., 1989). Nevertheless, granoblastic quartz and plagioclase evidence local high-temperature solid-state static recrystallization (Fig. 4C-D). Or else, secondary and bent twins also document medium-temperature solid-state deformation (Fig. 4E). Locally, more deformed rocks also record the local development of plagioclase porphyroclasts, core-and-mantle microstructures in feldspars, and subgrains suggesting medium- to high-temperature dynamic recrystallization (Fig. 4F).

4.4 Whole-rock geochemistry

4.4.1 Major elements

Whole-rock geochemistry were carried out in samples BA33-17, BA13-2-20, BA13-3-20, BA19-20 and SE8-19A). The igneous rocks of the Guillelmo-Serrucho Plutonic Complex have a silica content of ca. 45 – 60 wt. %, whereas Fe_2O_3 (total Fe), MgO and CaO lie between 5-12, 2-8 and 5-9 wt. %, respectively. The alcali content is low to intermediate (ca. 2.5-5% for Na_2O and 0.3-1.7% for K_2O) (Supplementary Material_1). In the TAS diagram (Middlemost, 1994; Fig 5A), samples plot mainly in gabbro-diorite to diorite fields and minor gabbro and granodiorite. Most samples correspond to the tholeiitic to calc- alkaline series according to the SiO_2 vs. K_2O diagram of Pecerillo and Taylor (1976) (Fig. 5B). The AFM diagram (Irvine and Baragar, 1971; Fig. 5C) depicts a similar trend, where calc-alkaline samples predominate over tholeiitic.

In the discrimination diagrams of Frost et al. (2001), samples are characterized by magnesian, metaluminous, and calcic to calc-alkalic composition (Figs. 5D-F). Thus, the batholith exhibits geochemical features comparable to those of Cordilleran granitoids.

4.4.2 Trace elements

The trace element diagram normalized to N-MORB (Sun and McDonough, 1989) shows an enrichment in LILE concerning HSFE (Fig. 6A). In general, all samples present a negative Nb anomaly and positive K and Pb anomalies. Nevertheless, Guillelmo lake samples seem to be less enriched in LILE than samples of other locations. The Cordón del Serrucho rocks exhibit a similar trend but seem the most enriched in trace elements (Fig. 6A)

Chondrite-normalized rare earth element diagram (Boynton, 1984) contents show a slight enrichment in LREE regarding HREE, which is clear in all samples (Fig. 6B). La_N/Yb_N ratio are low and vary between 1.55 (BA13-2-20, Guillelmo Lake) and 6.56 (SER-044, Cordón del Serrucho, Pankhurst et al., 2006). Samples of the Guillelmo lake are less enriched in REE than the remaining (Figure 6B). Moreover, there is a minor positive Eu anomaly in samples of the Guillelmo lake, with Eu/Eu* values varying between 1.12 and 1.40, whereas most of the samples from Cañadón de la Mosca and Cordón del Serrucho present a negligible to slightly positive anomaly in Eu, with Eu/Eu*, with values of 1.12.

The generally low Dy/Yb and Nb/Ta contents suggest the dominance of amphibole fractionation in the source (Fig. 7A-B; Fischer and Marty, 2005; Macpherson et al., 2006; Davidson et al., 2007; Ming Tang et al., 2019). Therefore, garnet in the source seems to be nearly absent, as further supported by relatively low La_N/Yb_N values. As documented by minor negative Ti anomalies, the fractionation of Ti-bearing phases may be feasible, though this process may be subordinate due to the low Nb/Ta values (Fig. 7C; John et al., 2011). On the other hand, the dominance of negligible to slightly positive Eu anomalies rules out plagioclase fractionation in the source. The slightly positive Eu/Eu* values may indicate very subordinate plagioclase accumulation (e.g., Dessimoz et al., 2012). The latter process, coupled with dominant amphibole fractionation, may thus account for the positive correlation between Eu/Eu* and Sr/Y (Fig. 7; Dessimoz et al., 2012; Oriolo et al., 2022).

As seen in the Nb/Yb vs. Th/Yb diagram of Pearce (2008) (Fig. 8), most samples deviate from the MORB-OIB array towards the volcanic arc array, with only one sample of the Guillelmo lake in the MORB-OIB field. The general trend indicates a MORB mantle source, possibly with a composition between N-MORB and E-MORB. This trend shows crustal components and may suggest possible metasomatism in the mantle source, if a slightly enriched source is assumed. In addition, the magmatic arc affinity is also supported by trace element patterns (Fig. 6) and discrimination diagrams of Pearce et al. (1984), where all the samples are located within the VAG field (Fig. 9).

4.5 Mineral chemistry and amphibole barometry

Amphibole mineral chemistry and barometry were carried out in samples BA 33-17 and SE8-19A of foliated diorites. Analytical results were analysed using the templated of Ridolfi (2021), whereas calibrations of Schmidt et al. (1992) and Mutch et al. (2016) were considered for barometric estimations (Fig. 10). There are no systematic variations within or between samples, with compositions corresponding to calcic amphiboles, namely tschermakite and magnesiohornblende, according to Leake et al. (1997) (Fig. 11).

Rocks of the Guillelmo-Serrucho Plutonic Complex have magnetite in its composition and, in fact, are ferromagnetic rocks. That is an important point for calibrations because they are based on oxygen fugacity (fO_2), with fO_2 above QFM (quartz-fayalite-magnetite) and below HM (hematite-magnetite) (Schmidt et al., 1992). Thus, the presence of magnetite ensures that it is working in a correct range of fO_2 for a correct use of the barometer.

According to the calibration of Schmidt et al. (1992), the obtained pressure for sample BA33-17 corresponds to a weighted average of 6.98 ± 0.31 kbar and, for sample SE8-19A, to a weighted average of 6.22 ± 0.18 kbar. On the other hand, pressures based on Mutch et al. (2016) yielded weighted average values of 5.40 ± 0.39 kbar for sample BA33-17 and 4.89 ± 0.18 kbar for sample SE8-19 . Both calibrations were also applied to experimental results of Mutch et al. (2016). Though both calibrations can be applied for plutonic rocks, there is less difference between experimental and calculated results using the Mutch et al. (2016) calibration than using the Schmidt et al. (1992) calibration. Therefore, pressure determinations based on Mutch et al. (2016) may be more representative for this study.

5. Discussion

5.1 The Guillelmo-Serrucho Plutonic Complex: a record of synorogenic primitive arc magmatism

The basement rocks in the study area have been classically considered amphibolites, as part of the Colohuincul or Bariloche Complex (Dalla Salda et al., 1991; García-Sansegundo et al., 2009; Oriolo et al., 2019). However, new geological, structural, microstructural, and geochronological evidence allows to separate this igneous body from the adjacent metasedimentary rocks.

In this regard, the “Guillelmo-Serrucho Plutonic Complex” is proposed to gather the middle to late Carboniferous intrusive bodies into a batholith cropping out between the Guillelmo lake region and the Cordón del Serrucho. Besides petrological and structural similarities, this correlation is further supported by ages of ca. 330-323 Ma revealed by U-Pb SHRIMP and LA-ICP-MS zircon data (Fig. 2; Pankhurst et al., 2006; Oriolo et al., 2022).

The batholith mainly comprises foliated diorites, quartz-diorites, and subordinate gabbros and tonalites. It presents well-defined magmatic foliation and lineation, compositional layering, and trails of mafic microgranular enclaves to a lesser extent and locally exhibits high-temperature solid- state microstructures related to cooling (Paterson et al., 1989), particularly at the northeastern margin of the pluton.

The widespread occurrence of NNW-SSE- to WNW-ESE-striking magmatic fabrics, which are comparable to metamorphic fabrics in the metasedimentary country rock (Fig. 3; Dalla Salda et al., 1991; García-Sansegundo et al., 2009; Oriolo et al., 2019), indicates a highly coupled system (Paterson et al., 1998; Paterson et al., 2019). Batholith emplacement thus occurred in an orogenic setting linked with transpressional deformation (García-Sansegundo et al., 2009; Oriolo et al., 2019). Field relationships and geochronological constrains show that the oldest intrusions (ca. 330 Ma) are rather felsic (e.g., Cordón del Serrucho quartz-diorites), though they show evidence of mingling, as documented by microgranular mafic enclaves. In addition, the late emplacement of more mafic intrusions at ca. 325-323 Ma suggest mafic magma replenishment. These observations thus point to incremental growth of batholith construction in less than ca. 10 My, possibly controlled by a regional ductile flow and transpressional deformation (e.g., Ingram and Hutton, 1994; Paterson and Miller, 1998; Miller and Paterson, 2001; Zak et al., 2009;

Pinotti et al., 2016). Further evidence is provided by thermobarometric data of the metasedimentary country rock, which shows a prograde path from ca. 6-8 to 10-12 kbar (Oriolo et al., 2019). Monazite EPMA Th-U-Pb data yielded ages of ca. 300 Ma for the timing of peak metamorphic conditions (or the subsequently decompression path), thus indicating a late Carboniferous age for the prograde path (Oriolo et al., 2019). Therefore, barometric results obtained for the Guillelmo-Serrucho Plutonic Complex, which are comparable to the early pressure estimations for the country rock P-T path, may roughly indicate an emplacement during the onset of transpressional progressive deformation of the Bariloche Complex.

On the other hand, geochemical data indicate a primitive arc composition and have features comparable to Cordilleran granitoids (Fig. 5D-F, Frost et al., 2001; Schmidt and Jagoutz, 2017, and references therein), showing an incipient continental crust signature. This is further supported by isotopic compositions, with values of Sr/Sr_0 of 0.704374 and 0.704625, εNd between -0,6 and 1.2 and εHf between 2.5 and 4.5 (Varela et al., 2005; Pankhurst et al., 2006; Fanning et al., 2011). The magmatic arc affinity is also supported by discrimination diagrams of Pearce et al. (1984) (Fig. 9). The slight deviation from the depleted mantle isotopic composition may indicate a slightly metasomatized source due to subduction, as evidenced by trace element data (Fig. 7). Alternatively, the crustal contribution might have resulted from minor assimilation of country rock during magma ascent and emplacement. In addition, barometric data coupled with the dominance of amphibole fractionation in the source (Section 4.5) points to middle/lower crustal depths resulting from the onset of the Gondwanide orogeny (Oriolo et al., 2022; see section 5.2).

On the other hand, the dominance of amphibole fractionation is clear according to low Dy/Yb and Nb/Ta contents (Fig. 7A-B; Fischer and Marty, 2005; Macphserson et al., 2006; Davidson et al., 2007; Ming Tang et al., 2019), while plagioclase seems to be very subordinate according to Eu/Eu* and Sr/Y (Fig. 7; e.g., Dessimoz et al. 2012). In addition, garnet in the source seems to be nearly absent, as further supported by relatively low La_N/Yb_N values. Minor negative Ti anomalies documented the feasible fractionation of Ti-bearing phases.

5.2 Petrotectonic context and regional implications

Following the early Carboniferous magmatic lull after widespread Devonian arc magmatism (e.g., Varela et al., 2005, 2015; Pankhurst et al., 2006; Hervé et al., 2016; Rapela et al., 2021; Oriolo et al., 2022), magmatism resumes at ca. 330 Ma in northern Patagonia, as documented by the Guillelmo-Serrucho Plutonic Complex. This early pulse at ca. 330-323 Ma represents the only primitive arc signature so far reported for the Gondwanide magmatism, as subsequent late Carboniferous to Permian intrusions is generally more evolved (e.g., Varela et al., 2005, 2015; Pankhurst et al., 2006; Oriolo et al., 2022). NW-SE magmatic structures in late Carboniferous-early Permian syntectonic granitoids, such as those recorded herein, match coeval NW-SE deformational fabrics in associated metamorphic rocks (Cerredo and López de Luchi, 1998; von Gosen, 2003, 2009; Giacosa et al., 2004; Oriolo et al., 2019; Renda et al., 2019, 2021). On a regional scale, igneous and metamorphic rocks delineate a NW-SE-striking regional belt, recording transpression and medium- to high-grade metamorphism in a continental magmatic arc (Renda et al., 2019, 2021; Oriolo et al., 2019; Marcos et al., 2020).

That magmatic arc has a NW-SE orientation in the Andean and extra-Andean Patagonian region of Argentina (Renda et al., 2019), whereas further northwest, it has a N-S orientation, mainly revealed by the Coastal Batholith of Chile (Fig. 12). The latter comprises calc-alkaline granitoids that were emplaced between ca. 320-300 Ma at ca. 35-40°S (Deckart et al., 2014). Though Gondwanide arc magmatism is also exposed further north, Alasino et al. (2022) showed two main age peaks at ca. 340 and 305 Ma associated with crustal thinning, which are succeeded by crustal thickening at ca. 280 Ma during the San Rafael Orogeny. This evolution contrasts significantly with that observed for northern Patagonia, where a magmatic gap is observed at ca. 340 Ma and synorogenic magmatism linked with crustal thickening is documented at ca. 330-300 Ma (e.g., Oriolo et al., 2019; Renda et al., 2019, 2021; Marcos et al., 2020), thus indicating a significant along-strike segmentation of the proto-Pacific marginal arc dynamics during the Carboniferous. Several coeval plutonic bodies are exposed between the northern North Patagonian Cordillera and the north-western North Patagonian Massif (Pankhurst et al., 2006; Varela et al., 2005, 2015; Hervé et al., 2013, 2018; Renda et al., 2019; Romero et al., 2019; Gregori et al., 2021; Oriolo et al., 2022). In the extra-Andean region, Renda et al. (2019) recognized multiples blocks of igneous-metamorphic rocks aligned in the NW-SE direction, where late Carboniferous plutons exhibit magmatic fabrics comparable to those recorded herein. Further intrusions in this area, such as the La Potranca leucogranite (289 ± 2 Ma; Pankhurst et al., 2006), present differences in the internal structure and are thus interpreted as post-tectonic granites (Renda et al., 2019).

In sum, magmatic fabrics indicate regional deformation during the emplacement (Renda et al., 2019). These syntectonic plutonic bodies were associated with the late Paleozoic Gondwanide active margin, documenting highly coupled magmatic systems at ca. 330-314 Ma (Fig. 12).

6. Conclusions

Paleozoic basement rocks in the study area (North Patagonian Andes, Argentina) are mainly diorites and quartz-diorites with subordinate gabbros. These rocks are assigned to the Guillelmo-Serrucho Plutonic Complex and contrast significantly with metasedimentary sequences of the Colohuincul or Bariloche Complex, which represent their wall rock.

The Guillelmo-Serrucho Plutonic Complex is characterized by widespread occurrence of NNWSSE- to WNW-ESE-striking magmatic fabrics, which indicate emplacement in a tectonically active setting. Similarities between these magmatic fabrics and those of the country rock indicate a highly coupled system, emplaced in an orogenic transpressional setting linked with the Gondwanide Orogeny. Field evidence, together with geochemical and geochronological data, suggest mafic magma replenishment during construction of a relatively large batholith (at least ca. 300 km^2) in a timespan of ca. <10 My. This batholith yields a primitive arc composition and documents the onset of Gondwanide subduction along the proto-Pacific margin of Gondwana.

The studied plutons are related to other bodies in the North Patagonian Andes and North Patagonian Massif, as well as plutonic bodies in Cordillera de la Costa of Chile, which are part of the Coastal Batholith. All these rocks have similar lithological, structural and geochemical characteristics, indicating widespread synorogenic arc pluton emplacement at ca. 330-314 Ma along the late Paleozoic Gondwanide active margin.

Acknowledgments

We are grateful for the help of Dr. Martin Robyr during microprobe analyses, Dr. Benita Putlitz and the Swiss Confederation for financial support. Sebastian Oriolo thanks financial support of the Nacional Geographic Society (grant CP-123R-17), Agencia Nacional de Promoción Científica y Tecnológica (PICT-2017-1092) and CONICET (PIP 11220200101662CO). We are also grateful to the Pablo Alasino and an anonymous reviewer for their comments and Andres Folguera for the editorial handling.

References

Alasino, P. H., Paterson, S. R., Kirsch, M., Larrovere, M. A., 2022. The role of crustal thickness on magma composition in arcs: An example from the pre-Andean, South American Cordillera. Gondwana Research, 106. 191-210.

Allmendinger, R. W., Cardozo, N., and Fisher, D., 2012. Structural geology algorithms: Vectors and tensors in structural geology. Cambridge University Press. 302.

Boynton, W. V., 1984. Chapter 3 - Cosmochemistry of the Rare Earth Elements: Meteorite Studies. Developments in Geochemistry. Vol 2, 63-114.

Cardozo, N., Allmendinger, R.W., 2013. Spherical projections with OSXStereonet. Computers & Geosciences. 51, 193-205.

Castro, A., Moreno-Ventas, I., Fernández, C., Vujovich, G., Gallastegui, G., Heredia, N., Martino, R.D., Becchio, R., Corretgé, L.G., Díaz-Alvarado, J., Such, P., García Arias, M., Liu, D. i., 2011. Petrology and SHRIMP U-Pb zircon geochronology of Cordilleran granitoids of the Bariloche area, Argentina. Journal of South American Earth Sciences. 32, 508-530.

Cawood, P.A., Leitch, E.C., Merle, R.E., Nemchin, A.A., 2011. Orogenesis without collision: Stabilizing the Terra Australis accretionary orogen, eastern Australia. GSA Bulletin, 123(11-12), 2240-2255.

Cerredo, M. E., López de Luchi, M. G., 1998. Mamil Choique Granitoids, southwestern North Patagonian Massif, Argentina: magmatism and metamorphism associated with a polyphasic evolution. J. S. Am. Earth Sci. 11 (5), 499-515.

Dahlquist, J. A., Alasino, P. H., Basei, M. A. S., 2018. Petrological, geochemical, isotopic, and geochronological constraints for the Late Devonian–Early Carboniferous magmatism in SW Gondwana (27–32°LS): an example of geodynamic switching. Int J Earth Sci (Geol Rundsch). 107, 2575–2603.

Dalla Salda, L., Cingolani, C., Varela, R., 1991. El basamento cristalino de la región norpatagónica de los lagos Gutiérrez, Mascardi y Guillelmo, provincia de Río Negro. Asociación Geológica Argentina. Rev. XLVI (3-4), 263-276.

Davidson, J., Turner, S., Handley, H., Macpherson, C., Dosseto. A., 2007. Amphibole “sponge” in arc crust? Geology. 35 (9): 787–790.

Deckart, K., Hervé, F., Fanning, M., Ramírez, V., Calderón, M., Godoy, E., 2014. U-Pb Geochronology and Hf-O Isotopes of zircons from the Pennsylvanian Coastal Batholith, South-Central Chile. Andean Geology. 41 (1): 49-82

Dessimoz, M., Müntener, O., Ulmer, P. A., 2012. A case for hornblende dominated fractionation of arc magmas: the Chelan Complex (Washington Cascades). Contrib Mineral Petrol 163. 567-589.

Fanning, C. M., Hervé, F., Pankhurst, R. J., Rapela, C. W., Kleiman, L. E., Yaxley, G. M., Castillo, P. (2011). Lu–Hf isotope evidence for the provenance of Permian detritus in accretionary complexes of western Patagonia and the northern Antarctic Peninsula region. Journal of South American Earth Sciences, 32(4), 485-496.

Mihai N. Ducea, Jason B. Saleeby and George Bergantz, 2015. The Architecture, Chemistry, and Evolution of Continental Magmatic Arcs. Annu. Rev. Earth Planet. Sci. 43:299-331.

Feruglio, E., 1947. San Carlos de Bariloche, Hoja 40b, escala 1:200.000. Carta Geológica-Económica de la Argentina. Dir. Geol. Min., (sin texto), Buenos Aires.

Fischer, T. P., Marty, B., 2005. Volatile abundances in the sub-arc mantle: insights from volcanic and hydrothermal gas discharges. Journal of Volcanology and Geothermal Research. Volume 140. Issues 1–3, Pages 205-216.

Franzese, J.R., 1995. El Complejo Piedra Santa (Neuquén, Argentina): parte de un cinturón metamórfico neopaleozoico del Gondwana suroccidental. Revista Geológica de Chile. Vol. 22, No. 2, 193-202.

Frost, R.B., Barnes, C., Collins, W., Arculus, R., Ellis, D. y Frost, C., 2001. A geochemical classification for granitic rocks. Journal of petrology. Vol. 42, No 11, 2033-2048.

García Sansegundo, J., Farias, P., Gallastegui, G., Giacosa, R.E. y Heredia, N., 2009. Structure and metamorphism of the Gondwanan basement in the Bariloche region (North Patagonian Argentine Andes). Geology Reserch. 98, 1599–1608.

Giacosa, R. E., Heredia, N., Zubía, M. A., González, R., Faroux, A., Césari, O., Franchi, M., 2001. Hoja Geológica 4172-IV, San Carlos de Bariloche. Hoja Geológica BRC.

Giacosa, R. E., Heredia, C., 2002. Hoja Geológica 4172-IV, San Carlos de Bariloche. Provincias de Río Negro y Neuquén. Instituto de Geología y Recursos Minerales, Servicio Geológico Minero Argentino. Boletín 279, 77.

Giacosa, R. E., Heredia, N., 2004. Structure of the North Patagonian thick-skinned fold-and-thrust belt, southern central Andes, Argentina (41°–42° S). Journal of South American Earth Sciences. 18, 61–72.

Gill, J.B., 1981. Bulk Chemical Composition of Orogenic Andesites. In: Orogenic Andesites and Plate Tectonics. Minerals and Rocks, vol 16. Springer, Berlin, Heidelberg.

González Bonorino, F., 1944. Descripción geológica y petrográfica de la Hoja 41 b, Río Foyel (territorio de Río Negro). Boletín de la Dirección de Minas, Geología e Hidrología. 56, 124.

Gregori, D. A., Strazzere, L., Barros, M., Benedini, L., Marcos, P., & Kostadinoff, J., 2021. The Mencué batholith: permian episodic arc-related magmatism in the western North Patagonian Massif, Argentina. International Geology Review. 63(3), 317-341.

Hervé, M., Suarez, M., Puig, A., 1984. The Patagonian Batholith S of Tierra del Fuego, Chile: timing and tectonic implications. Journal of the Geological Society. Volume 141, Pages 909 - 917

Hervé, F., Calderón, M., Fanning, C.M., Pankhurst, R.J. y Godoy, E., 2013. Provenance variations in the Late Paleozoic accretionary complex of central Chile as indicated by detrital zircons. Gondwana Research. 23, 1122–1135.

Hervé, F., Calderón, M., Fanning, C.M., Pankhurst, R.J., Fuentes, F., Rapela, C.W., Correa, J., Quezada, P. y Marambio, C., 2016. Devonian magmatism in the accretionary complex of southern Chile. Journal of the Geological Society.

Hervé, F., Calderon, M., Fanning, C. M., Pankhurst, R. J., Rapela, C. W., & Quezada, P. (2018). The country rocks of Devonian magmatism in the north Patagonian massif and Chaitenia. Andean Geology. 45(3), 301–317.

Ingram, G. M., Hutton, D. H., 1994. The Great Tonalite Sill: Emplacement into a contractional shear zone and implications for Late Cretaceous to early Eocene tectonics in southeastern Alaska and British Columbia. Geological Society of America Bulletin. 106(5), 715-728.

Irvine, T.N. and Baragar, W. R. A, 1971. A Guide to the Chemical Classification of the Common Volcanic Rocks. Canadian Journal of Earth Sciences. Volume 8, Number 5.

Janoušek, V., Farrow, C.M., Erban, V., 2006. Interpretation of whole-rock geochemical data in igneous geochemistry: introducing Geochemical Data Toolkit (GCDkit). J. Petrol. 47, 1255–1259.

Janoušek, V., Moyen, J.-F., Martin, H., Erban, V., Farrow, C., 2016. Geochemical Modelling of Igneous Processes – Principles and Recipes in R Language. Springer, Berlin Heideberg.

John, T., Klemd, R., Klemme, S., Pfänder, J. A., Elis Hoffmann, J., Gao, J., 2011. Nb–Ta fractionation by partial melting at the titanite–rutile transition. Contributions to Mineralogy and Petrology. 161(1), 35-45.

Kleiman, L. E., Japas, M. S., 2019. The Choiyoi volcanic province at 34°S-36°S (San Rafael, Mendoza, Argentina): implications for the late Palaeozoic evolution of the southwestern margin of Gondwana. Tectonophysics. 473, 283-299.

Leake BE, Woolley AR, Arps CES, Birch WD, Gilbert MC, Grice JD, Hawthorne FC, Kato A, Kisch HJ, Krivovichev VG, Linthout K, Larid J, Mandarino JA, Maresch WV, Nickel EH, Rock NMS, Schumacher JC, Smith DC, Stephenson NCN, Ungaretti L, Whittaker EJW, Guo Y, 1997. Nomenclature of amphiboles: report of the subcommittee on amphiboles of the International Mineralogical Association, Comission on New Minerals and Minerals Names. Can mineral 35:219-246.

Llambías, E.J., Kleiman, L.E., and Salvarredi, J.A., 1993. El magmatismo gondwánico. XII Congreso Geológico Argentino y II Congreso de Exploración de Hidrocarburos. Relatorio I (6), 53-64.

Llambías, E. J., Rapela, C.W., 1984. Geología de los complejos eruptivos de La Esperanza, provincia de Río Negro. Revista de la asociación geológica argentina XXXIX (3-4), 220-243.

Llambías, E. J., 2003. Geología de los cuerpos ígneos. Asociación Geológica Argentina. 27, Buenos Aires, 182.

Lucassen, F., Trumbull, R., Franz, G., Creixell, C., Vásquez, P., Romer, L.F. y Figueroa, O., 2004. Distinguishing crustal recycling and juvenile additions at active continental margins: the Paleozoic to recent compositional evolution of the Chilean Pacific margin (36–41°S). Journal of South American Earth Sciences. 17, 103–119.

Macpherson, C.G., Dreher, S.T., Thirlwall. M.F., 2006. Adakites without slab melting: high pressure differentiation of island arc magma, Mindanao, the Philippines. Earth Planet. Sci. Lett. 243, 581-593

Marcos, P., Pavón Pivetta, C., Benedini, L., Gregori, D.A., Geraldes, M., Scivetti, N., Barros, M., Varela, M., Costa Dos Santos, A, 2020. Late Paleozoic geodynamic evolution of the western North Patagonian Massif and its tectonic context along the southwestern Gondwana margin. Lithos.

Marschall, H. R., Schumacher, J. C., 2012. Arc magmas sourced from mélange diapirs in subduction zones. Nature Geoscience. 5(12), 862-867.

Middlemost, E.A.K., 1994. Naming materials in the magma/igneous rock system. Earth Sci. Rev. 37, 215-224

Miller, R. B., Paterson, S. R., 2001. Construction of mid-crustal sheeted plutons: Examples from the North Cascades, Washington. Geological Society of America Bulletin. 113(11), 1423-1442.

Ming Tang, Wei-Qiang Ji, Xu Chu, Anbin Wu, Chen Chen, 2020. Reconstructing crustal thickness evolution from europium anomalies in detrital zircons. Geology. 49 (1): 76–80.

Oriolo, S., Schulz, B., González, P., Bechis, F., Olaizola, E., Krause, J., Renda, E., Vizán, H., 2019. The late Paleozoic tectonometamorphic evolution of Patagonia revisited: insights from the pressure-temperature-deformation-time (P-T-D-t) path of the Gondwanide basement of the North Patagonian Cordillera (Argentina). Tectonics 38, 2378-2400.

Oriolo et al. 2022. Earth and Planetary Science Letters

Pankhurst, R.J., Rapela, C.W., Fanning, C.M. y Márquez, M., 2006. Gondwanide continental collision and the origin of Patagonia. Earth-Science Reviews 76, 235–257.

Paterson, S. R., Ardill, K., Vernon, R., Žák, J., 2008. A review of mesoscopic magmatic structures and their potential for evaluating the hypersolidus evolution of intrusive complex. Journal of Structural Geology. 125, 134-147.

Paterson, S. R., Miller, R. B., 1989. Magma emplacement during arc-perpendicular shortening: An example from the Cascades crystalline core, Washington. Tectonics, volume 17, issue 4, 571-586.

Paterson, S., Veron, R. y Tobisch, O., 1989. A review of criteria for the identification of magmatic and tectonic foliations in granitoids. Journal of Structural Geology. Vol. 11. No 3, 349 – 363.

Paterson, S. R., Miller, R. B., 1998. Mid-crustal magmatic sheets in the Cascades Mountains, Washington: implications for magma ascent. Journal of Structural Geology. 20(9-10), 1345-1363.

Paterson, S. R., Fowler, Jr., T. K., Schmidt, K. L., Yoshinobu, A. S., Yuan, E. S., & Miller, R. B., 1998. Interpreting magmatic fabric patterns in plutons. Lithos. 44(1-2), 53-82.

Paterson, S.R., Ardill, K., Vernon, R., Žák, J., 2019. A review of mesoscopic magmatic structures and their potential for evaluating the hypersolidus evolution of intrusive complexes. J. Struct. Geol. 125, 134-147.

Pearce, J. A., Harris, N. B. W., Tindle, A. G., 1984. Trace Element Discrimination Diagrams for the Tectonic Interpretation of Granitic Rocks. *Journal of Petrology*. Volume 25, Issue 4, 956–983.

Pearce, J.A., 2008. Geochemical fingerprinting of oceanic basalts with applications to ophiolite classification and the search for Archean oceanic crust. Lithos. 100, 14-48

Peccerillo, A., Taylor, S.R., 1976. Geochemistry of Eocene calc-alkaline volcanic rocks from the Kastamonu area, Northern Turkey. Contr. Mineral. and Petrol. 58, 63–81.

Pinotti, L. P., D'Eramo, F. J., Weinberg, R. F., Demartis, M., Tubía, J. M., Coniglio, J. E., Aragon, E., 2016. Contrasting magmatic structures between small plutons and batholiths emplaced at shallow crustal level (Sierras de Córdoba, Argentina). Journal of Structural Geology. 92, 46-58.

Proserpio, C. A., 1978. Descripción geológica de la hoja 42D, Gastre, Provincia de Chubut. Servicio Nacional Minero Geológico 159.

Ramos, A. V., 2008. Patagonia: A paleozoic continent adrift? Journal of South American Earth Sciences. 26, 235–251.

Rapela, C. W., Hervé, F., Pankhurst, R. J., Calderón, M., Fanning, C. M., Quezada, P., Poblete, F., Palape, C., Reyes, T., 2021. The Devonian accretionary orogen of the North Patagonian cordillera. Gondwana Res. 96, 1-21

Ravazzoli, I., Sesana, F., 1977. Descripción geológica de la Hoja 41 c Río Chico. Boletín Servicio Geológico Nacional, 148, Buenos Aires.

Renda, E. M., Álvarez, D., Prezzi, C., Oriolo, S. y Vizán, H., 2019. Inherited basement structures and their influence in foreland evolution: A case study in Central Patagonia, Argentina. Tectonophysics. 772.

Renda, E. M., González, P. D., Vizán, H., Oriolo, S., Prezzi, C., Ruiz González, V., Schulz, B., Krause, V., Basei, M., 2021. Igneous-metamorphic basement of Taquetrén Range, Patagonia, Argentina: A key locality for the reconstruction of the paleozoic evolution of Patagonia. J. S. Am. Earth Sci. 106, Article 103045

Ridolfi, F., 2021. Amp-TB2: An Updated Model for Calcic Amphibole Thermobarometry. Minerals. 11, 324.

Romero, R., Barra, F., Leisen, M., Salazar, E., González-Jiménez, J. M., Reich, M., 2019. Sedimentary provenance of the Late Paleozoic metamorphic basement, south-central Chile:

Implications for the evolution of the western margin of Gondwana. International Geology Review.

Santonja C., Bechis F., Suriano J., Falco J. I., Encinas A., Olaizola E.R., Valencia V. A., Litvak V. D., Ramos, V. A., 2021. Tectono-stratigraphic evolution of the northeastern sector of the Ñirihuau basin, north Patagonian Andes, Argentina: Insights from sedimentology and geochronology data of the Ñirihuau formation. J. South Am. Earth Sci. 111, Article 103487

Sato, A., Llambías, E., Basei, M., and Castro, C., 2015. Three stages in the Late Paleozoic to Triassic magmatism of southwestern Gondwana, and the relationships with the volcanogenic events in coeval basins: Journal of South American Earth Sciences. V. 63, p. 48–69.

Schmidt, M. W., Jagoutz, O., 2017. The global systematics of primitive arc melts. Geochemistry, Geophysics, Geosystems. 18(8), 2817-2854.

Serra-Varela, S., Heredia, N., Otamendi, J., Giacosa, R., 2021. Petrology and geochronology of the San Martín de los Andes batholith: Insights into the Devonian magmatism of the North Patagonian Andes. Journal of South American Earth Sciences. Volume 109, 103-283, ISSN 0895-9811.

Sun, S. and McDonough, W. F., 1989. Chemical and isotopic systematics of oceanic basalts: implications for mantle composition and processes. Geological Society, London, Special Publications. Volume 42, 313 - 345.

Turner, J. C. M., 1965. Estratigrafía de la comarca Junin de los Andes (Neuquén). Acad. Nac. Ciencias. Bol 44, 5-51, Cordoba.

Varela, R., Teixeira, W., Cingolani, C., and Dalla Salda, L., 1994. Edad Rubidio-Estroncio de granitoides de Aluminé-Rahue, Cordillera Norpatagónica, Neuquén, Argentina, in VII Congreso Geológico Chileno: Concepción, Actas, p. 1254–1258.

Varela, R., Basei, M., Cingolani, C., Siga, O. y Passarelli, C., 2005. El basamento cristalino de los Andes norpatagónicos en Argentina: geocronología e interpretación tectónica. Revista Geológica de Chile. Vol. 32, No. 2, 167-187.

Varela, R., Gregori, D.A., Gonzales, P.D. y Basei, M., 2015. Caracterización geoquímica del magmatismo de arco devónico y carbonífero-pérmico en el noroeste de Patagonia, Argentina. Revista de la Asociación Geológica Argentina. 72 (3), 419 -432.

Volkheimer, W., 1964. Estratigrafía de la zona extraandina del Departamento de Cushamen (Chubut) entre los paralelos 42° y 42°30’ y los meridianos 70° y 71°. Asoc. Geol. Argentina. Rev. 19(2), 85-107, Buenos Aires.

Von Gosen, W., 2003. Thrust tectonics in the North Patagonian Massif (Argentina): implications for a Patagonia plate. Tectonics. 22(1), 1005.

Von Gosen, W., 2009. Stages of Late Palaeozoic deformation and intrusive activity in the western part of the North Patagonian Massif (southern Argentina) and their geotectonic implications. Geological Magazine, 146(1), 48-71.

Žák, J., Paterson, S., Janoušek, V., Kabele, P., 2009. The Mammoth Peak sheeted complex, Tuolumne batholith, Sierra Nevada, California: a record of initial growth or late thermal contraction in a magma chamber? Contributions to Mineralogy and Petrology. 158(4), 447.

Table 1. Samples, type rock, localities and geological area and zircon U-Pb geochronological data included in the map of Figure 1. References: 1. Pankhurst et al. (2006); 2. Romero et al. (2019); 3. Oriolo et al. (2022); 4. Renda et al. (2021). (NPM: North Patagonian Massif; NPC: North Patagonian Cordillera; PCN: Precordillera Neuquina).

Figure 1. Regional sketch map modified from Pankhurst et al. (2006) and Oriolo et al. (2019). Zircon U-Pb SHRIMP and LA-ICP-MS data of Carboniferous to Permian intrusions are also included (see Table 1 for further details).

Figure 2. Geological map with structural data of the studied area (modified after Feruglio, 1947; González Bonorino, 1944; Giacosa and Heredia, 2001; Varela et al., 2005; Pankhurst et al., 2006; García Sansegundo et al., 2009; Santonja et al., 2021). Ages taken from Pankhurst et al. (2006) and Varela et al. (2015). Lower hemisphere equal area projections of poles of magmatic foliation (black dots) and lineation (red dots) are shown. Data of metamorphic foliation of the country rock (Bariloche Complex) is shown in the red diagram.

Figure 3. Magmatic foliated rocks present in the study area. Amphibole and plagioclase crystals define the foliation at the Guillelmo lake margins (A) and the Cañadón de la Mosca area (B). C. Elongated microgranular mafic enclaves subparallel to foliation. D-E. Compositional layering at Morro de Sheffield and Guillelmo lake zones, respectively.F. Magmatically folded and faulted mafic layering (schlieren) at Cordón del Serrucho zone.

Figure 4. Photomicrographs (crossed polars). A. Shape-preferred orientation of hornblende (Hbl) and plagioclase (Pl) crystals defining the magmatic foliation. B. Magmatic compositional layering. C-D. Polygonal granoblastic quartz (C)-plagioclase (D) aggregates, indicated by arrows. E. Secondary twinning and bent in plagioclase. F. Sub-grains and core-and-mantle microstructure with recrystallized tails (arrow) in plagioclase porphyroclast.

Figure 5. A. TAS diagram (Middlemost, 1994). B. SiO_2 vs. K_2O diagram (Pecerillo and Taylor, 1976). C. AFM diagram (Irvine and Baragar, 1971). D, E, F. Discrimination diagrams of Frost et al. (2001). Grey dots: Guillelmo lake (BA 33-17; BA 13-2-20; BA 13-3-20; BA 19-20; Dalla Salda et al., 1991; Varela et al., 2005; García-Sansegundo et al., 2009), red dots: Cordón del Serrucho and Río Ternero (SE 8-19A; Pankhurst et al., 2006; García-Sansegundo et al., 2009), green dots: Cañadón de la Mosca (Pankhurst et al., 2006; Varela et al., 2005).

Figure 6. A. Spider diagram normalized to NMORB (Sun and McDonough, 1989); B. REE spider diagram normalized to chondrite (Boynton, 1984). Grey dots: Guillelmo lake (BA 33-17; BA 13-2-20; BA 13-3-20; BA 19-20; Varela et al., 2005; García-Sansegundo et al., 2009), red dots: Cordón del Serrucho and Río Ternero (SE 8-19A; Pankhurst et al., 2006; García-Sansegundo et al., 2009), green dots: Cañadón de la Mosca (Pankhurst et al., 2006; Varela et al., 2005).

Figure 7. Diagrams of Dy/Yb vs. SiO_2 (A), Sr/Y vs. Eu/Eu* (B) and Nb/Ta vs. SiO_2 (C). Grey dots: Guillelmo lake (BA 33-17; BA 13-2-20; BA 13-3-20; BA 19-20; Varela et al., 2005; García-Sansegundo et al., 2009), red dots: Cordón del Serrucho and Río Ternero (SE 8-19A; Pankhurst et al., 2006; García-Sansegundo et al., 2009), green dots: Cañadón de la Mosca (Pankhurst et al., 2006; Varela et al., 2005).

Figure 8. Nb/Yb vs. Th/Yb diagram by Pearce (2008). (OIB: Ocean Island Basalt; E-MORB: Enriched Middle Ocean Ridge Basalt; N-MORB: Normal Middle Ocean Ridge Basalt). Grey dots: Guillelmo lake (BA 33-17; BA 13-2-20; BA 13-3-20; BA 19-20; Varela et al., 2005; García-Sansegundo et al., 2009), red dots: Cordón del Serrucho and Río Ternero (SE 8-19A; Pankhurst et al., 2006; García-Sansegundo et al., 2009), green dots: Cañadón de la Mosca (Pankhurst et al., 2006; Varela et al., 2005).

Figure 9. Granite tectonic discrimination diagram of Pearce et al. (1984). (ORG: Ocean Ridge Granites; VAG: Volcanic Arc Granites; WPG: Within Plate Granites; syn-COLG: Syncollisional Granites). Grey dots: Guillelmo lake (BA 33-17; BA 13-2-20; BA 13-3-20; BA 19-20; Varela et al., 2005; García-Sansegundo et al., 2009), red dots: Cordón del Serrucho and Río Ternero (SE 8-19A; Pankhurst et al., 2006; García-Sansegundo et al., 2009), green dots: Cañadón de la Mosca (Pankhurst et al., 2006; Varela et al., 2005).

Figure 10. Microprobe image and representative profile of amphibole crystal of sample SE 8-19A, which shows no systematic variation in pressure.

Figure 11. Amphibole classification figure. Values correspond to tschemakite and magnesiohornblende according to fields defining by Leake et al. (1997).

Figure 12. Sketch map reconstructing the late Carboniferous-early Permian Gondwanide magmatic arc in northern Patagonia (ages come from Pankhurst et al., 2006; Deckart et al., 2014; Renda et al., 2019).

Samples	*Rock*	*Locality*	*Region*	*Age (Ma)*	*Ref*
PIC-216	Pichiñanes Granite	Sa. de los Pichiñanes	NPM	318 ± 2	1
SAP 210	Paso del Sapo foliated Granodiorite	Paso del Sapo	NPM	314 ± 2	1
G1	Paso del Sapo Plutonic Complex tonalite	Paso del Sapo	NPM	314.1 ± 2.2	4
GAS 025	Laguna del Toro Granodiorite	Gastre	NPM	293 ± 2	1
PLA-049	El Platero Tonalite	El Maiten	NPM	329 ± 4	1
MAC-128	Mamil Choique Formation	Sa. Mamil Choique	NPM	281 ± 2	1
CUS-130	El Tunel Tonalite	Río Chico	NPM	295 ± 2	1
SE 8-19A	Guillelmo-Serrucho Plutonic Complex diorite	Morro de Shieffeld	NPC	324 ± 2	3
SER-044	Guillelmo-Serrucho Plutonic Complex diorite	Cordón del Serrucho	NPC	330 ± 4	1
MOS-043	Guillelmo-Serrucho Plutonic Complex diorite	Cañadón de la Mosca	NPC	323 ± 3	1
BA33_17	Guillelmo-Serrucho Plutonic Complex diorite	Lago Guillelmo	NPC	325 ±4	3
RRPS-1	Chachil Plutonic Complex granite	Chachil	PCN	303 ± 2	2
RA 5-18	Chachil Plutonic Complex granite	Cuesta de Rahue	PCN	300 ± 2	3
RA 10-18	Chachil Plutonic Complex granite	Rahue	PCN	305 ± 2	3
RA 48-18	Chachil Plutonic Complex granite	Catán Lil creek	PCN	358 ± 2	3

Table 1. Samples, type rock, localities and geological area and zircon U-Pb geochronological data included in the map of Figure 1. References: 1. Pankhurst et al. (2006); 2. Romero et al. (2019); 3. Oriolo et al. (2022); 4. Renda et al. (2021). (NPM: North Patagonian Massif; NPC: North Patagonian Cordillera; PCN: Precordillera Neuquina).

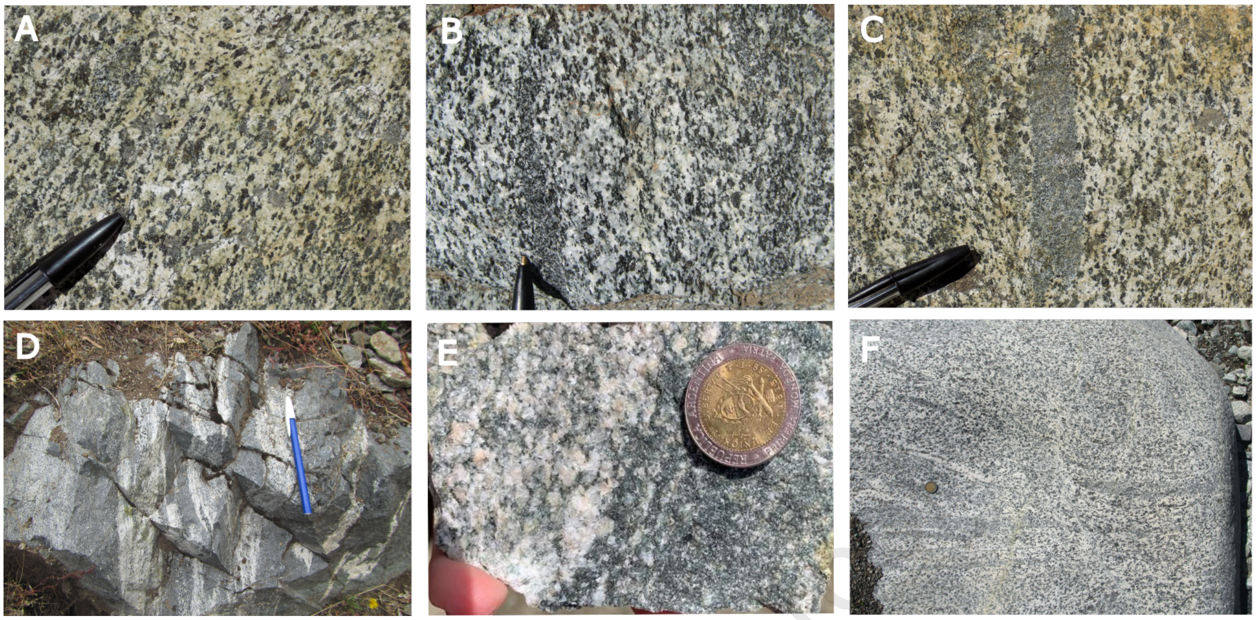
A
B
C
D
E
F

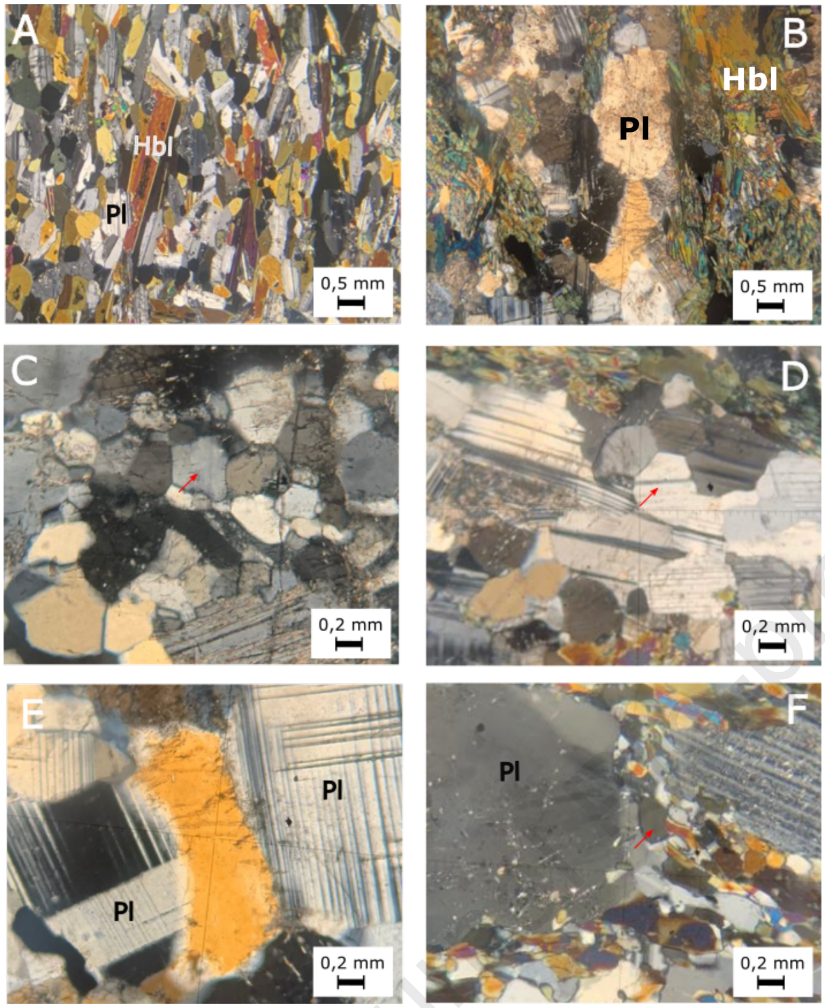
A
Hbl
Pl
0,5 mm
B
Hbl
Pl
0,5 mm
C
0,2 mm
D
0,2 mm
E
Pl
Pl
0,2 mm
F
Pl
0,2 mm

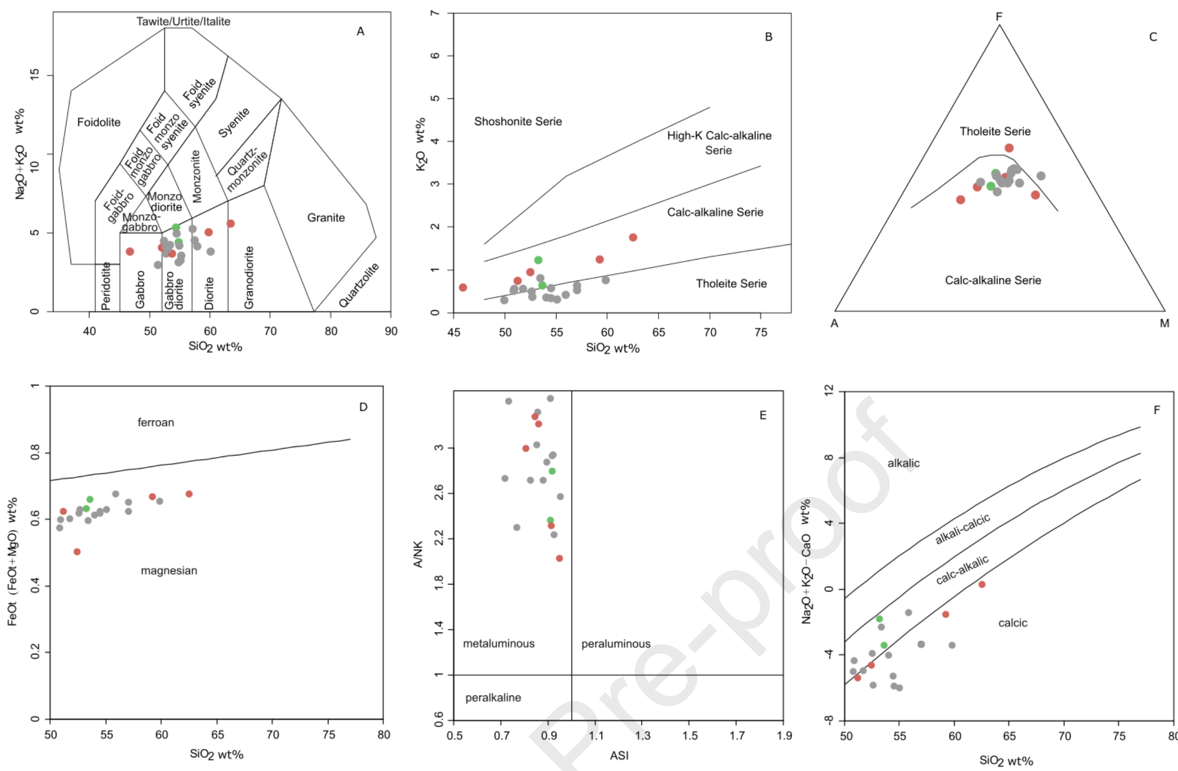

Tawite/Urtite/Italite
A
Foidolite
Foid gabbro
Foid monzo gabbro
Foid monzo syenite
Foid syenite
Syenite
Monzo diorite
Monzo-gabbro
Monzonite
Quartz-monzonite
Granite
Quartzolite
Peridotite
Gabbro
Gabbro diorite
Diorite
Granodiorite
Na2O+K2O wt%
SiO2 wt%
B
Shoshonite Serie
High-K Calc-alkaline Serie
Calc-alkaline Serie
Tholeite Serie
K2O wt%
C
F
A
M
Tholeite Serie
Calc-alkaline Serie
D
ferroan
magnesian
FeOt (FeOt+MgO) wt%
E
metaluminous
peraluminous
peralkaline
A/NK
ASI
F
alkalic
alkali-calcic
calc-alkalic
calcic
Na2O+K2O−CaO wt%

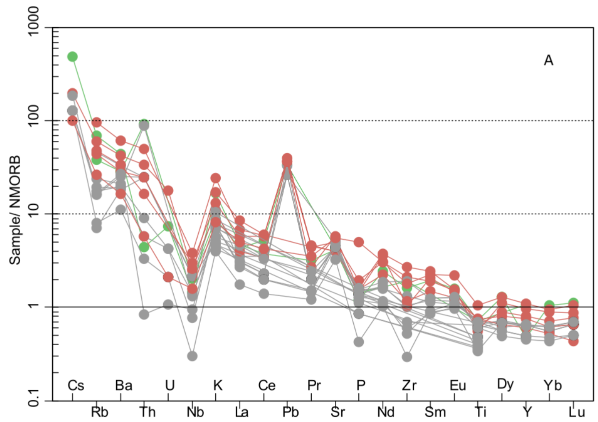
A
Sample/ NMORB
0.1
1
10
100
1000
Cs
Rb
Ba
Th
U
Nb
K
La
Ce
Pb
Pr
Sr
P
Nd
Zr
Sm
Eu
Ti
Dy
Y
Yb
Lu

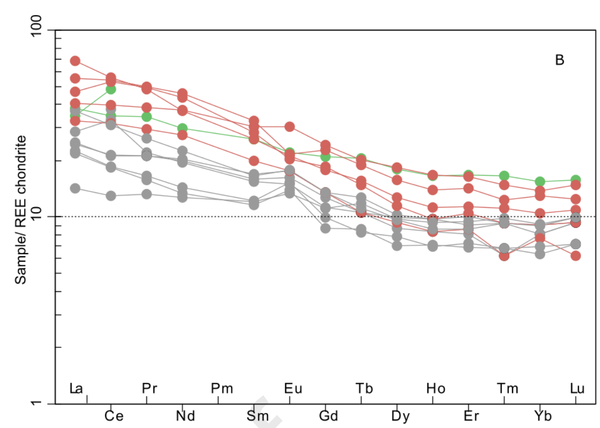
B
Sample/ REE chondrite
1
10
100
La
Ce
Pr
Nd
Pm
Sm
Eu
Gd
Tb
Dy
Ho
Er
Tm
Yb
Lu

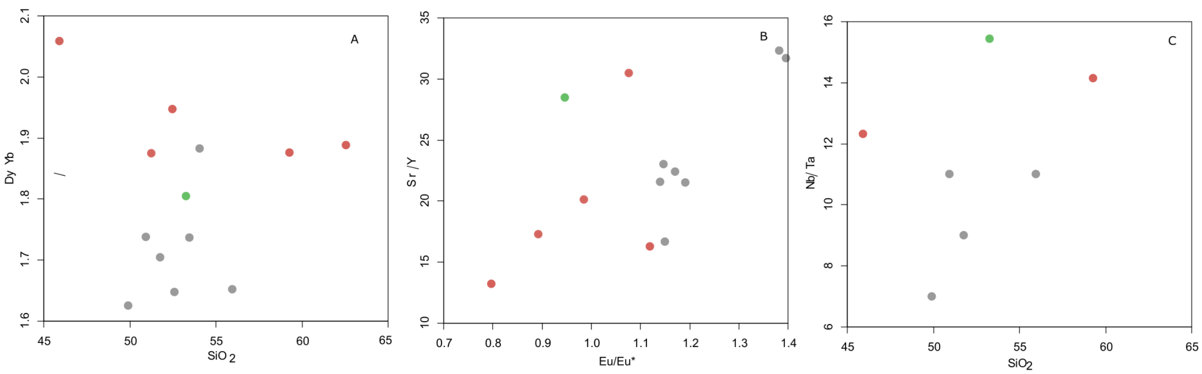
A
Dy Yb
SiO 2
B
Sr /Y
Eu/Eu*
C
Nb/ Ta
SiO2

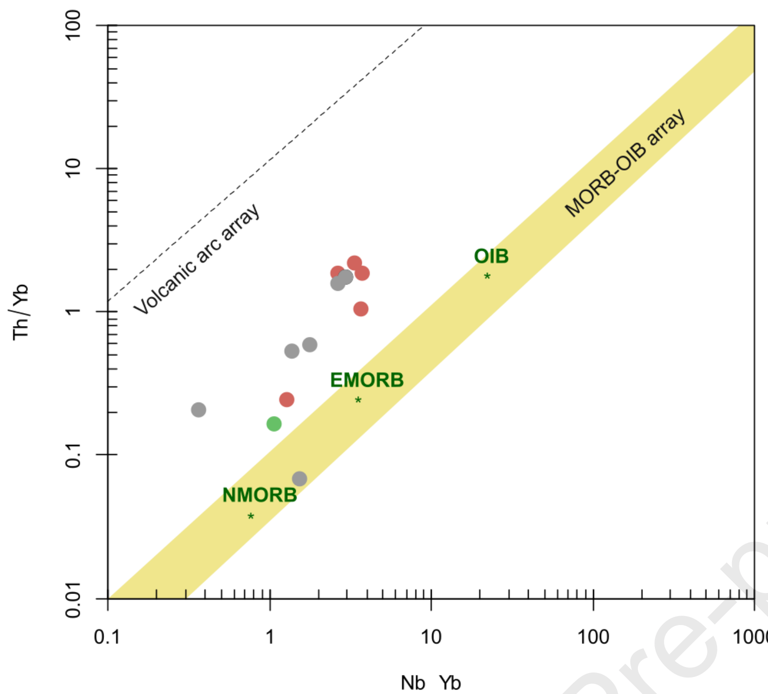

Th/Yb
100
10
1
0.1
0.01
0.1
1
10
100
1000
Nb Yb
Volcanic arc array
MORB-OIB array
OIB
EMORB
NMORB

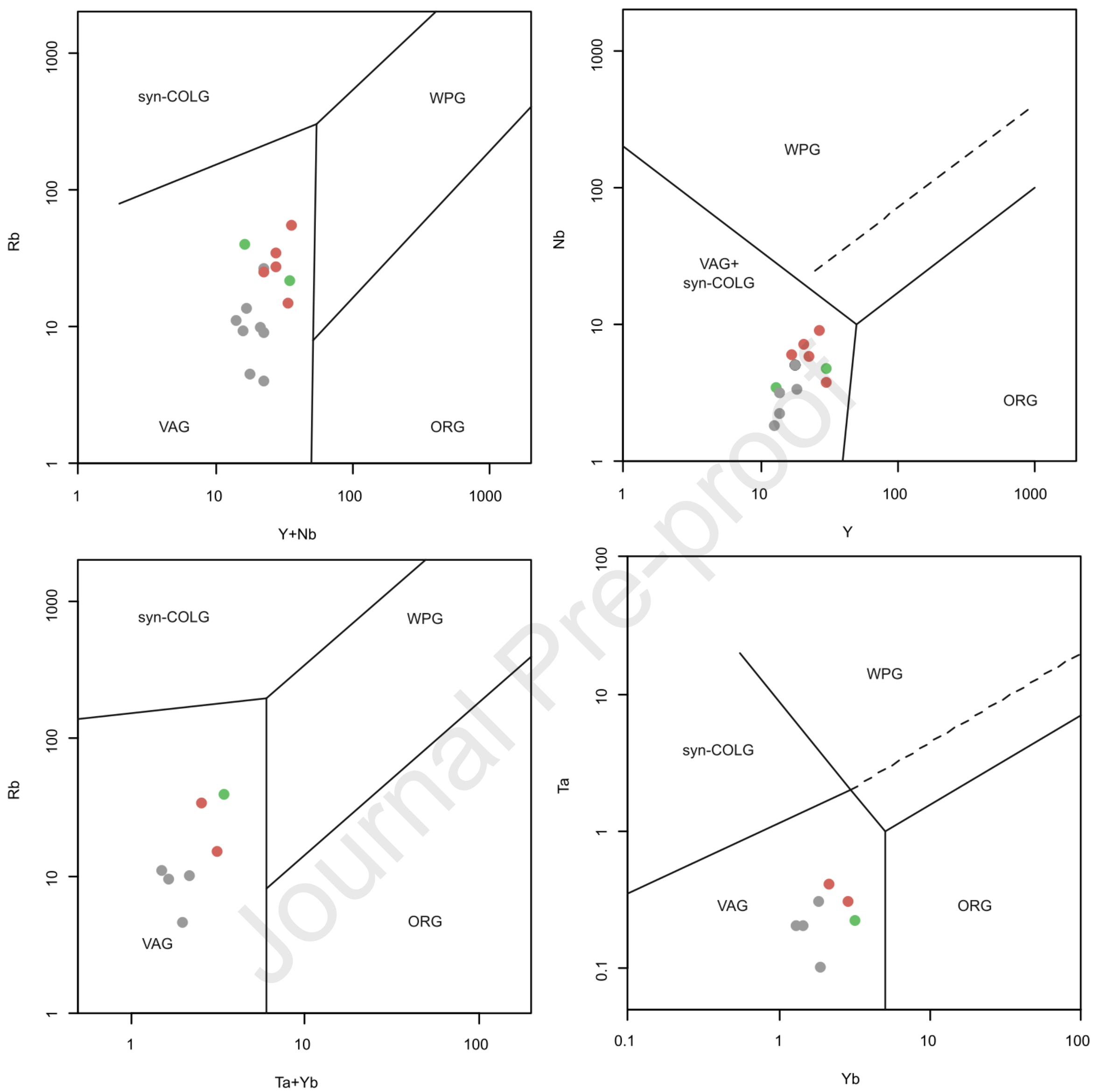
syn-COLG
WPG
VAG
ORG
Rb
Y+Nb
1
10
100
1000
WPG
VAG+
syn-COLG
ORG
Nb
Y
syn-COLG
WPG
VAG
ORG
Rb
Ta+Yb
WPG
syn-COLG
VAG
ORG
Ta
Yb
0.1

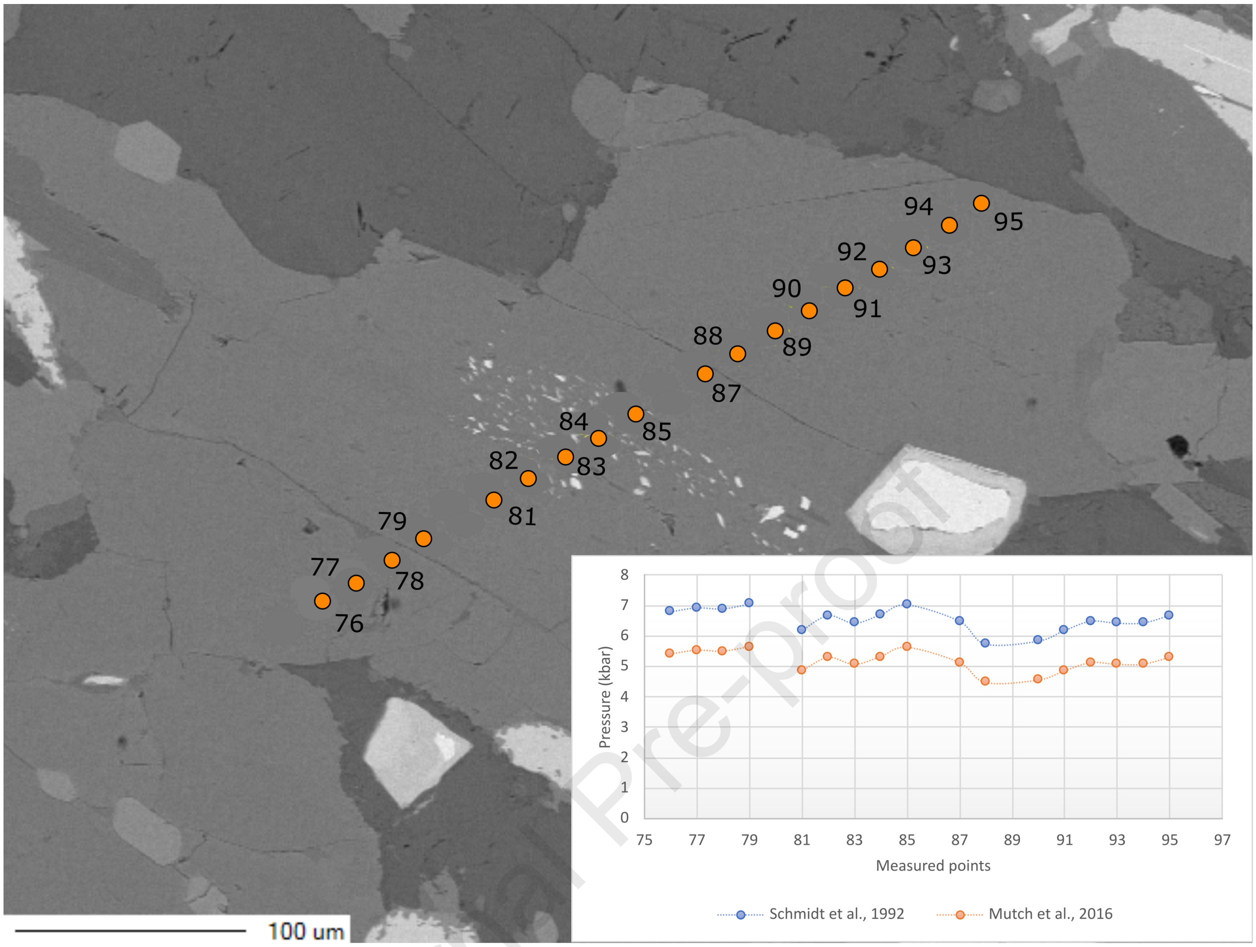

94
95
92
93
90
91
88
89
87
84
85
82
83
79
81
77
78
76
100 um
Pressure (kbar)
Measured points
Schmidt et al., 1992
Mutch et al., 2016

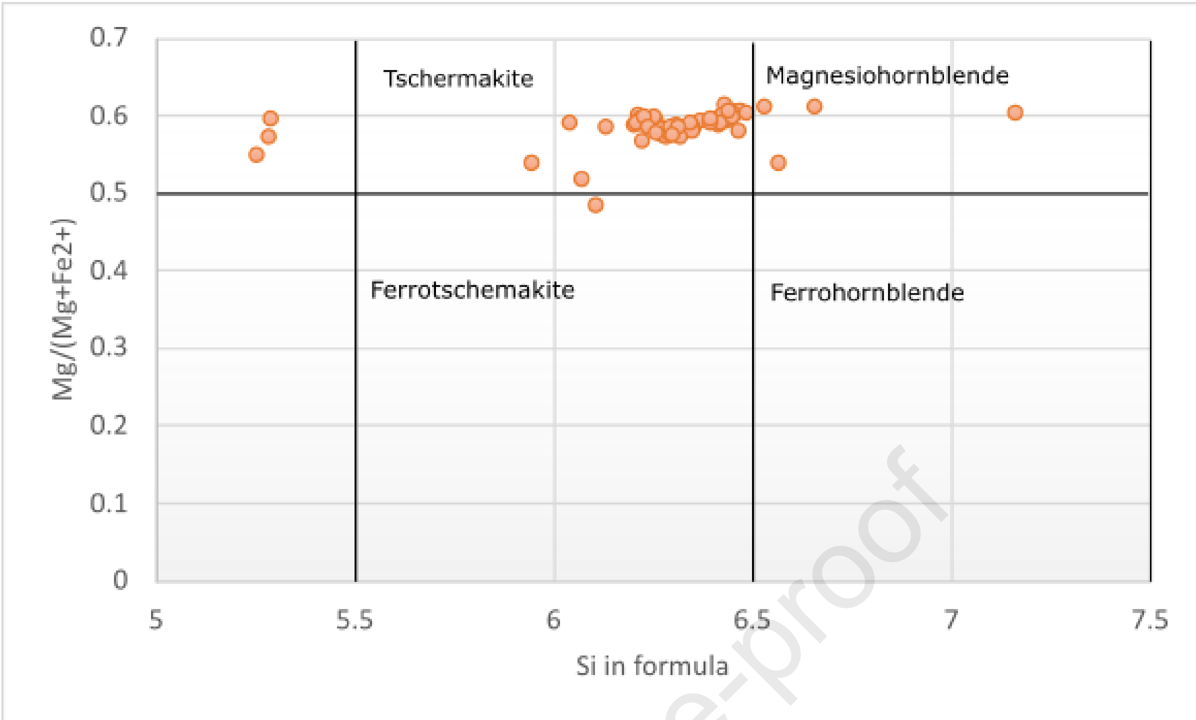

0.7
0.6
0.5
0.4
0.3
0.2
0.1
0
Mg/(Mg+Fe2+)
5
5.5
6
6.5
7
7.5
Si in formula
Tschermakite
Magnesiohornblende
Ferrotschemakite
Ferrohornblende


-72.000
-69.000
-36.000
-39.000
-42.000
References
Localities and ages
Study zone
Constitución
300 ± 2 Ma
Concepción
310 ± 2.5 Ma
303 ± 2 Ma
Lago Aluminé
305 ± 2 Ma
358 ± 2 Ma
300 ± 2 Ma
Valdivia
San Martín de los Andes
325 ± 4 Ma
Lago Guillelmo
323 ± 3 Ma
Cañadón de la Mosca
330 ± 4 Ma
Cordón del Serrucho
Morro de Shieffeld
324 ± 2 Ma
El Platero
329 ± 4 Ma
Paso del Sapo
314 ± 2 Ma
Sa. de los Pichiñanes
318 ± 2 Ma
CHILE
ARGENTINA
0
50
100 km
La Potranca
289 ± 2 Ma

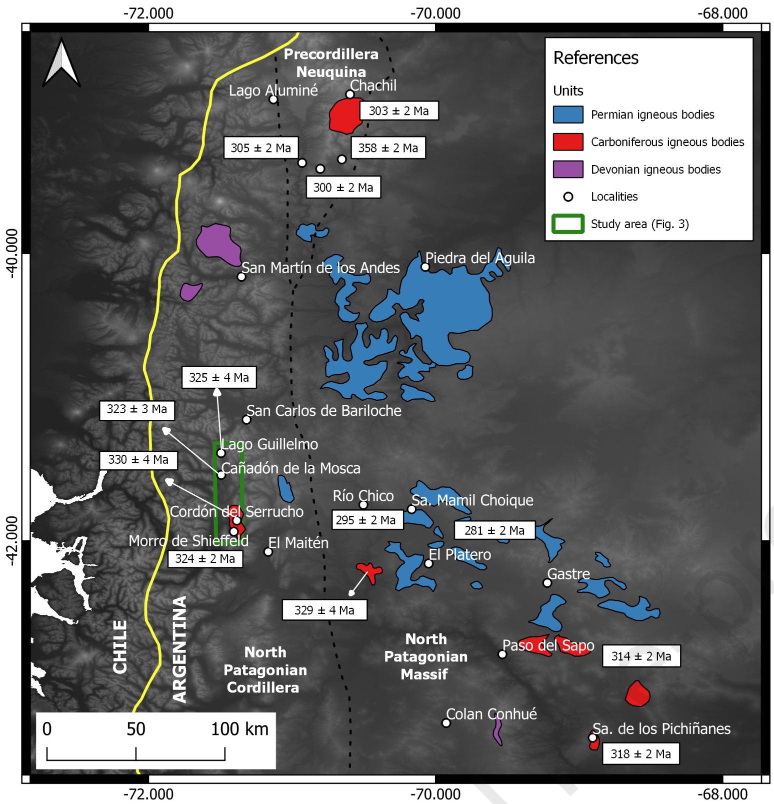
-72.000
-70.000
-68.000
-40.000
-42.000
References
Units
Permian igneous bodies
Carboniferous igneous bodies
Devonian igneous bodies
Localities
Study area (Fig. 3)
Precordillera Neuquina
Lago Aluminé
Chachil
303 ± 2 Ma
305 ± 2 Ma
358 ± 2 Ma
300 ± 2 Ma
San Martín de los Andes
Piedra del Aguila
325 ± 4 Ma
323 ± 3 Ma
San Carlos de Bariloche
Lago Guillelmo
330 ± 4 Ma
Cañadón de la Mosca
Río Chico
Sa. Mamil Choique
295 ± 2 Ma
281 ± 2 Ma
Cordón del Serrucho
Morro de Shieffeld
324 ± 2 Ma
El Maitén
El Platero
Gastre
329 ± 4 Ma
CHILE
ARGENTINA
North Patagonian Cordillera
North Patagonian Massif
Paso del Sapo
314 ± 2 Ma
Colan Conhué
Sa. de los Pichiñanes
318 ± 2 Ma
0
50
100 km

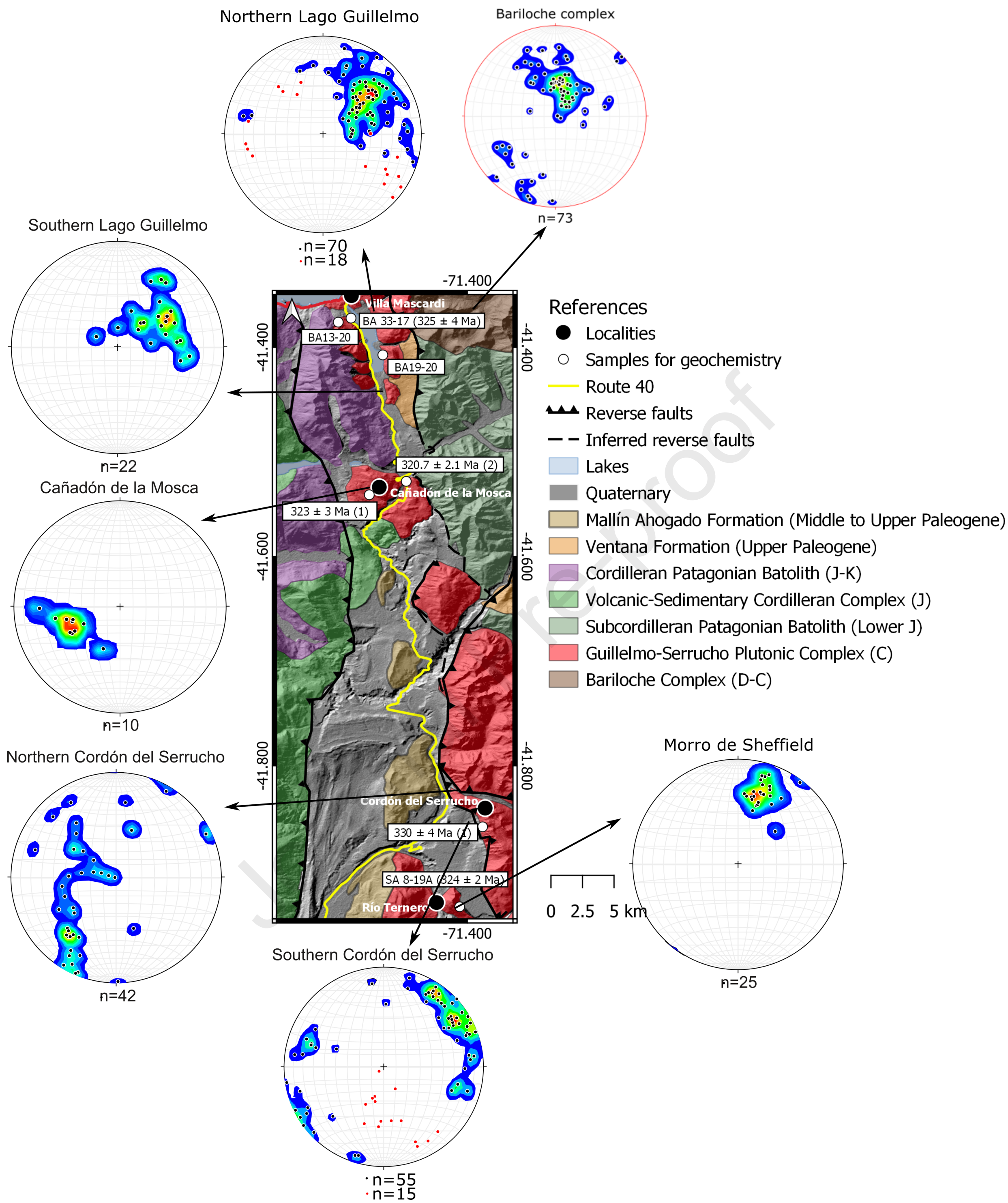
Northern Lago Guillelmo
n=70
n=18
Bariloche complex
n=73
Southern Lago Guillelmo
n=22
Cañadón de la Mosca
n=10
Northern Cordón del Serrucho
n=42
Southern Cordón del Serrucho
n=55
n=15
Morro de Sheffield
n=25
-71.400
-41.400
-41.600
-41.800
Villa Mascardi
BA 33-17 (325 ± 4 Ma)
BA13-20
BA19-20
320.7 ± 2.1 Ma (2)
Cañadón de la Mosca
323 ± 3 Ma (1)
Cordón del Serrucho
330 ± 4 Ma (1)
SA 8-19A (324 ± 2 Ma)
Río Ternero
References
Localities
Samples for geochemistry
Route 40
Reverse faults
Inferred reverse faults
Lakes
Quaternary
Mallín Ahogado Formation (Middle to Upper Paleogene)
Ventana Formation (Upper Paleogene)
Cordilleran Patagonian Batolith (J-K)
Volcanic-Sedimentary Cordilleran Complex (J)
Subcordilleran Patagonian Batolith (Lower J)
Guillelmo-Serrucho Plutonic Complex (C)
Bariloche Complex (D-C)
0 2.5 5 km

1. Basement rocks of the North Patagonian Massif are studied.
2. Guillelmo-Serrucho Plutonic Complex is defined.
3. Whole-rock geochemistry and mineral chemistry data is analyzed.
4. A petrotectonic context and regional implications is discussed.
5. Sketch map reconstructing the Gondwanide magmatic arc in northern Patagonia (C-P) is presented.

Declaration of interests

☒ The authors declare that they have no known competing financial interests or personal relationships that could have appeared to influence the work reported in this paper.

☐The authors declare the following financial interests/personal relationships which may be considered as potential competing interests: